



# Ex Vivo Maturation of 3D-Printed, Chondrocyte-Laden, Polycaprolactone-Based Scaffolds Prior to Transplantation Improves Engineered Cartilage Substitute Properties and Integration

CARTILAGE  
2022, Vol. 13(4) 105–118  
© The Author(s) 2022  
DOI: 10.1177/19476035221127638  
journals.sagepub.com/home/CAR  
SAGE

Carlos M. Chiesa-Estomba<sup>1,2\*</sup>, Raquel Hernández-Moya<sup>3,4\*</sup> , Claudia Rodiño<sup>5</sup>, Alba Delgado<sup>5</sup>, Gonzalo Fernández-Blanco<sup>6</sup>, Javier Aldazabal<sup>6</sup>, Jacobo Paredes<sup>6</sup>, Ander Izeta<sup>3,4,6,7</sup> , and Ana Aiastui<sup>3,4,5</sup>

## Abstract

**Objective.** The surgical management of nasal septal defects due to perforations, malformations, congenital cartilage absence, traumatic defects, or tumors would benefit from availability of optimally matured septal cartilage substitutes. Here, we aimed to improve *in vitro* maturation of 3-dimensional (3D)-printed, cell-laden polycaprolactone (PCL)-based scaffolds and test their *in vivo* performance in a rabbit auricular cartilage model. **Design.** Rabbit auricular chondrocytes were isolated, cultured, and seeded on 3D-printed PCL scaffolds. The scaffolds were cultured for 21 days *in vitro* under standard culture media and normoxia or in prochondrogenic and hypoxia conditions, respectively. Cell-laden scaffolds (as well as acellular controls) were implanted into perichondrium pockets of New Zealand white rabbit ears ( $N = 5$  per group) and followed up for 12 weeks. At study end point, the tissue-engineered scaffolds were extracted and tested by histological, immunohistochemical, mechanical, and biochemical assays. **Results.** Scaffolds previously matured *in vitro* under prochondrogenic hypoxic conditions showed superior mechanical properties as well as improved patterns of cartilage matrix deposition, chondrogenic gene expression (*COL1A1*, *COL2A1*, *ACAN*, *SOX9*, *COL10A1*), and proteoglycan production *in vivo*, compared with scaffolds cultured in standard conditions. **Conclusions.** *In vitro* maturation of engineered cartilage scaffolds under prochondrogenic conditions that better mimic the *in vivo* environment may be beneficial to improve functional properties of the engineered grafts. The proposed maturation strategy may also be of use for other tissue-engineered constructs and may ultimately impact survival and integration of the grafts in the damaged tissue microenvironment.

## Keywords

3D bioprinting, additive manufacturing, cartilage, chondrogenic differentiation, scaffold maturation

## Introduction

Surgical reconstruction of nasal cartilage defects may be approached by prefabricated flaps and tissue expanders. However, surgeons often need use of a limited number of donor sites in the body, such as costal or auricular cartilage, which (1) may not be adequate to fulfill the defect, (2) may not have the same functional characteristics as the target cartilage tissue, and (3) may be associated with significant morbidity risks.<sup>1</sup> Therefore, a number of tissue engineering strategies are being explored for cartilage regeneration, mostly at the preclinical level.<sup>2–5</sup> Among these, 3-dimensional (3D) bioprinting of cartilage substitutes presents the advantage of being tailor-made for each patient's defect,

thus providing as yet another example of personalized medicine.<sup>6–15</sup> Of note, it is relevant to consider criteria such as the size, shape, and biological and mechanical properties of the nasal cartilage for successful (i.e. functional) tissue reconstruction.<sup>16</sup> Among many possible materials to be used as a scaffold for nasal cartilage reconstruction, polycaprolactone (PCL) seems suitable as it is an absorbable and porous material which has been used in numerous clinical applications,<sup>17</sup> including rhinoplasty.<sup>18,19</sup> Furthermore, PCL-based scaffolds have tunable properties,<sup>20</sup> and their biocompatibility and long-term efficacy and safety in humans are well known.<sup>21</sup> Cell-free materials could theoretically be used to restore damaged cartilage tissue and provide a scaffold for endogenous cell proliferation onto



focal defects. However, most studies on the *in vivo* performance of cell-free scaffolds have yielded unsatisfactory results.<sup>22</sup> For these reasons, the field is now focused on the development of diverse types of cell-laden constructs for cartilage repair.

On the cellular side, many studies have focused on proving biocompatibility of available scaffolds, with no particular attention to chondroinductive potential of used materials.<sup>23</sup> However, it is well known that chondrocytes dedifferentiate in expansion culture,<sup>24</sup> and therefore, use of alternative cell sources (for instance, articular cartilage progenitor cells)<sup>25</sup> or strategies for re-differentiation of chondrocytes prior to transplantation<sup>26</sup> seem advisable. Since the pioneering studies of Hollander comparing nasal and articular chondrocytes for tissue engineering applications,<sup>27</sup> the field has advanced a great deal and diverse cell sources have been explored for cartilage regeneration.<sup>28</sup> Most studies have focused on the use of mesenchymal stromal cells (MSCs) of diverse origins.<sup>29,30</sup> However, MSC multipotency entails the possibility of alternative adipose or osteogenic differentiation.<sup>31</sup> Other research groups have used culture-expanded nasal<sup>32-34</sup> or auricular<sup>35</sup> chondrocytes or have compared diverse heterotopic chondrocyte sources.<sup>36</sup>

In this study, we aimed to improve rabbit chondrocyte-laden, PCL-based scaffolds maturation and test their *in vivo* performance in a rabbit auricular cartilage model. To this end, we exposed the scaffolds to prochondrogenic media *in vitro*. As cartilage is avascular and presents a low oxygen tension microenvironment, we tested hypoxic versus normoxic culture conditions. To simulate the septal cartilage environment, a rabbit ear surgery protocol was selected due to the low morbidity and high reliability of the structure to simulate the clinical conditions to test the scaffold. We further analyzed the *in vitro* and *in vivo* behavior of the scaffolds, their mechanical properties, and their chondrogenic potential *in vivo*.

## Methods

### Animal Welfare

Twenty adult 2.0- to 2.5-kg New Zealand white rabbits were included. They were housed with access to water and

nourishment *ad libitum* under pathogen-free conditions in barrier facilities of the Biodonostia Health Research Institute. Rabbits were housed 1 animal per cage under diary observation to assess their welfare during the study period (12 weeks).

### Scaffold Design and Synthesis

Scaffolds were designed using Creo Parametric 3D Modeling Software v4.0 (PTC products). The first layer was composed of 9 cylinders of 10.35 mm length and 0.15 mm thickness separated 1 mm between them. The second layer presented 11 cylinders of 8.25 mm length and 0.15 mm thickness separated 1 mm between them, transversal to the underlying layer. To provide an elliptic form, the outermost 2 cylinders at each side were shortened in curvature. Scaffolds with 4, 8, and 16 layers were designed by copy-pasting the 2-layered construct. PCL scaffolds were 3D-printed using fused deposition modeling (FDM) technology on a Biobots 1 bioprinter (Allevi, Philadelphia, PA). PCL polymer (Polycaprolactone Bioink Kit, Allevi) was introduced into the bioprinter syringe, melted by heating to 100 °C and subsequently dispensed through a 27G metal needle, using a pressure of 100 PSI and a deposition speed of 0.1 mm/seg. Printed scaffolds were sterilized by soaking in 70% ethanol for 1 hour and exposed to ultraviolet (UV) lamp irradiation for 30 minutes.

### Rabbit Chondrocyte Isolation and Expansion

Briefly, rabbit ear cartilage was obtained *post mortem* after removing hair, skin, and perichondrium of the tissue. Cartilage fragments were sliced in small pieces and transferred onto multiwell plates where they were rinsed with washing medium (Hank's balanced salt solution [HBSS, Gibco], supplemented with 2% Penicillin/Streptomycin [P/S] and 2% Fungizone™ [Gibco]). Tissue fragments were digested in digestion medium (Dulbecco's Modified Eagle Medium [DMEM, Sigma-Aldrich] containing 1.5 mg/ml of Collagenase type II [Gibco] and 2% P/S plus 2% Fungizone™) overnight at 37 °C, with gentle shaking. Cells were filtered through a 70-µm nylon cell strainer (Corning)

<sup>1</sup>Department of Otorhinolaryngology-Head and Neck Surgery, Osakidetza, Donostia University Hospital, San Sebastián, Spain

<sup>2</sup>Otorhinolaryngology and Head and Neck Surgery Group, Biodonostia Health Research Institute, San Sebastián, Spain

<sup>3</sup>Multidisciplinary 3D Printing Platform, Biodonostia Health Research Institute, San Sebastián, Spain

<sup>4</sup>ISCIII Platform of Biobanks and Biomodels, Instituto de Salud Carlos III (ISCIII), Madrid, Spain

<sup>5</sup>Histology Platform, Biodonostia Health Research Institute, San Sebastián, Spain

<sup>6</sup>Department of Biomedical Engineering and Sciences, School of Engineering, Tecnun-University of Navarra, San Sebastián, Spain

<sup>7</sup>Tissue Engineering Group, Biodonostia Health Research Institute, San Sebastián, Spain

\*These authors contributed equally to this work.

### Corresponding Authors:

Ander Izeta, Tissue Engineering Group, Biodonostia Health Research Institute, Paseo Doctor Begiristain s/n, 20014 San Sebastián, Spain.

Email: [ander.izeta@biodonostia.org](mailto:ander.izeta@biodonostia.org)

Ana Aiastui, Multidisciplinary 3D Printing Platform, Biodonostia Health Research Institute, Paseo Doctor Begiristain s/n, 20014 San Sebastián, Spain.

Email: [ana.aiastui@biodonostia.org](mailto:ana.aiastui@biodonostia.org)

in order to get rid of undigested tissue fragments and aggregations. Cells were centrifuged at 1,500 rpm for 5 minutes and washed 3 times with washing medium. The cells were then resuspended in expansion medium (low glucose DMEM supplemented with 10% fetal bovine serum [FBS; Gibco™] and 1% P/S). Viable cells were determined using trypan blue dye exclusion technique. Isolated chondrocytes were cultured until confluence at 37 °C in a humidified CO<sub>2</sub> incubator, replacing the medium every 3 days.

### **In Vitro Cell-Laden 3D Scaffold Maturation**

A total amount of 50,000 auricular chondrocytes were seeded on top of the scaffolds allowing them to adhere and grow for 1 week in expansion medium in a humidified CO<sub>2</sub> incubator, changing medium twice a week. At this specific point, half of the scaffolds were kept in expansion medium and normoxic (21% O<sub>2</sub>) atmosphere, while the other half were cultured under hypoxic conditions (1% O<sub>2</sub>) with pro-chondrogenic medium (High Glucose DMEM [Sigma-Aldrich], 5% FBS [Gibco], 1x Insulin-Transferrin-Selenium [ITS; Gibco], 100 nM dexamethasone, 100 µg/ml ascorbic acid, 1% P/S, 400 mM glutamine [Sigma-Aldrich], 10 ng/ml transforming growth factor-beta 2 [TGF-β2; Peprotech]) for 3 weeks. Samples were taken at days 7, 14, and 21 of culture. The matured scaffolds in both conditions were implanted into rabbits at day 21 of culture.

### **Biochemical Evaluation of Neocartilage Formation and Quantification of DNA Content and Cell Viability**

Three samples of each condition and time were digested with 4 U/ml Papain at 60 °C overnight in phosphate buffered saline (PBS, Gibco) containing 6 mM of L-Cysteine hydrochloride and 6 mM of ethylenediaminetetraacetic acid disodium salt solution (all from Sigma-Aldrich). Total sulfated glycosaminoglycans (sGAG) were quantified using Blyscan Glycosaminoglycan Assay (Biocolor) according to the manufacturer's instructions. Absorbance was measured at 656 nm in a HALO LED 96 microplate reader (Dynamica). Total DNA content was measured in the same digested samples used for sGAG assay following the protocol of Quant-iT™ dsDNA High-Sensitivity Assay kit (Life Technologies). DNA yield was measured at an excitation wavelength of 485 nm and an emission wavelength of 528 nm in an Appliskan plate reader (Thermo). The viability of the seeded cells was qualitatively assessed using a Live/Dead kit (Invitrogen). Scaffolds collected at specified time points were washed with PBS (Gibco) for 5 minutes. Next, a staining solution of ethidium homodimer and Calcein AM in PBS was added to each well and incubated at 37 °C for 45 minutes, followed by several washes with PBS. Images were taken with a Nikon 80i fluorescence microscope.

### **In Vivo Assay**

For rabbit ear surgery, after the skin incision, a perichondrium pocket was designed. A circle shape biopsy of elastic cartilage of 1 cm of diameter was extracted without penetrating the lateral skin. The generation of perichondrium pocket allowed us to simulate the cartilage environment. In the case of the defect group (*Control-Ct*; *N* = 5 ears), the wound was closed without any kind of insert or scaffold. In the rest of the cases, the gap generated in the tissue was refilled with acellular scaffolds (*Acellular-Ac*; *N* = 5), scaffolds with chondrocytes cultured in non-prochondrogenic conditions in normoxia (*Normoxia-No*; *N* = 5), and scaffolds with chondrocytes cultured in prochondrogenic conditions in hypoxia (*Hypoxia-Hy*; *N* = 5). To control sepsis all along the experiment, early markers of sepsis and inflammation were monitored every 14 days. Thus, blood samples were collected from the jugular vein of anesthetized rabbits and sent to the Biochemistry Service of Donostia University Hospital to determine C-reactive protein (CRP) and procalcitonin serum levels. At study end point (12 weeks), rabbits were sacrificed and grafted tissues were extracted.

### **Histological Assessments: Staining and Immunofluorescence**

Tissue cryosections (7 µm thick) were sliced in a cryostat and fixed for staining. Glycosaminoglycan (GAG) content was visualized by Alcian Blue-Safranin O staining. For immunohistochemistry, tissue sections were blocked with FBS (Gibco) and bovine serum albumin (BSA, Sigma). Sections were incubated with primary antibodies anti-type I (AB90395, Abcam) and anti-type II (1320-01, Southern Biotech) collagens. Secondary antibodies Alexa Fluor 488 and 555 were added at 1:500 dilution and incubated for 1 hour at room temperature. Sections were analyzed using a Fluorescence Microscope Nikon 80i.

### **RNA Extraction and Reverse Transcription-Quantitative Polymerase Chain Reaction (RT-qPCR) Analysis**

For the *in vitro* experiments, total RNA was isolated from the scaffolds of each condition at days 7, 14, and 21 of culture. For scaffolds analyzed after extraction from the *in vivo* setting, tissues from surgical areas of each condition were recovered (with 0.5-1 cm of margin around the inserted scaffold/cartilage/defect) from the ears of the sacrificed rabbits at study end point. Tissues or scaffolds were frozen and lysed with buffer RLT (Qiagen) containing β-mercaptoethanol. RNA extractions were carried out with RNeasy Mini Kit and RNeasy Plus Micro Kit (Qiagen) for the *in vivo* and *in vitro* experiments, respectively. A total of 1 ng of RNA was reverse transcribed into complementary DNA by using High-Capacity

RNA to DNA kit (Applied Biosystems). Then, cDNA was pre-amplified using TaqMan® PreAmp Master Mix according to the manufacturer instructions. Quantitative real-time PCR was performed using TaqMan® Expression Master Mix and the following TaqMan assay primers: *ACAN* (Oc06726465\_m1), *COL1A1* (Oc03396073\_g1), *COL2A1* (Oc03396134\_m1), *COL10A1* (Oc04097225\_s1), and *SOX9* (Oc04096872\_m1). The reaction was carried out in a CFX384 Touch Real-Time PCR Detection System with the following cycling parameters: 50°C for 2 minutes, 95°C for 10 minutes for polymerase activation, and 40 cycles of 15 seconds at 95°C for denaturation plus 1 minute at 60°C for annealing. Results were analyzed using  $2^{-\Delta Ct}$  method relative to *GAPDH* housekeeping gene primers (Oc03823402\_g1), in the case of *in vitro* samples, or  $2^{-\Delta\Delta Ct}$  method (relative to control group), in the case of *in vivo* samples.

### Scanning Electron Microscopy (SEM)

A Philips XL30 CP (Amsterdam, The Netherlands) SEM was used to observe the scaffolds and cells morphology with an acceleration voltage of 15 kV and different magnifications. Briefly, scaffolds were washed 3 times with Dulbecco's phosphate-buffered saline (DPBS) and fixed with glutaraldehyde 2.5% plus paraformaldehyde 2% in PBS for 90 minutes at room temperature. Samples were then dehydrated in graded ethanol and air-dried after their immersion in hexamethyldisilane (HMDS, Sigma-Aldrich) for 10 minutes. Finally, they were coated with a few nanometers of Palladium (SC7620 Mini Sputter Coater).

### Mechanical Analysis by Uniaxial Compression Tests

Uniaxial tests were carried out on a ZwickiLine Z1.0 testing machine (Zwick/Roell, Ulm, Germany). The load cell used was a 50 N Zwick/Roell Xforce P (Zwick/Roell). The software for controlling the machine and recording data was the Zwick/Roell testXpert III v1.4 with all patches installed up to the sx406-218-5. The toll used for performing the compression tests was homemade and consists of 2 aluminum cylinders. From these experiments, the Young's modulus was calculated for each sample.

### Statistical Analysis

IBM SPSS Statistics 24 (Armonk, NY) was used. After running the Shapiro-Wilk test, in case of the normal distribution of the results, 1-way analysis of variance (ANOVA) tests were used. For the *post hoc* analysis, Bonferroni was applied in the case of homoscedasticity; on the contrary, Games-Howell non-parametric test was used. In cases of non-parametric data, for the ANOVA, the Kruskal-Wallis test was performed.

## Results

### PCL Scaffold Printing and Rabbit Chondrocyte Seeding

To develop 3D-printed PCL scaffolds, parallel meshed structures composed of 2, 4, 8, and 16 layers were designed and their printability at 100 °C was tested, excluding the possibility of printing with live cells (**Fig. 1**). Considering rabbit ears' size (where the scaffolds were to be implanted), the chosen scaffold thickness was 2-layer, with a resolution of 0.1 mm in height and a nozzle diameter of 0.15 mm. To cellularize 3D-printed PCL scaffolds with rabbit auricular chondrocytes, sterilized scaffolds were incubated with chondrocytes in the presence of standard expansion medium under normoxic conditions or in the presence of prochondrogenic medium under hypoxic conditions. After 21 days of maturation in culture, the mature cell-laden scaffolds as well as controls were implanted in perichondrium pockets of rabbits' ears, and their evolution was followed up for a period of 12 weeks.

### 3D Culture and In Vitro Chondrogenic Differentiation

**Biochemical characterization of neocartilage formation.** To test biocompatibility of the PCL scaffolds with rabbit chondrocytes and to determine the best incubation period and culture conditions to induce cartilage regeneration, a live/dead assay was performed at days 7, 14, and 21 of culture (**Fig. 2**). Occasionally, a few dead cells were observed at day 7 in both hypoxia and normoxia conditions (red cells in **Fig. 2A** and **B**, respectively). However, the overall majority of cells were alive (green) and healthily attached to the scaffold surfaces. In fact, an increase of attached live cells was especially apparent at days 14 and 21 of hypoxia conditions (**Fig. 2C** and **E**) compared with normoxic conditions (**Fig. 2D** and **F**).

Quantification of total sGAG demonstrated increased extracellular matrix (ECM) deposition by day 21, with no significant differences between study groups. Maximum sGAG values deposited on the scaffolds were  $38.78 \pm 7.99$   $\mu\text{g/ml}$  in hypoxic conditions compared with  $29.07 \pm 4.00$   $\mu\text{g/ml}$  in normoxia, perhaps indicating a tendency of prochondrogenic media and hypoxia to induce increased ECM deposition (**Fig. 2G**). Significant differences were only obtained between days 0 and 21 in both normoxic and hypoxic conditions ( $P = 0.042$  and  $P = 0.013$ , respectively).

As varying cell numbers may affect the amount of sGAG deposited in the scaffolds, sGAG values were normalized to DNA content. In this analysis, scaffolds matured in hypoxia showed again a tendency to increase sGAG secretion compared with normoxia (**Fig. 2H**), but significant differences

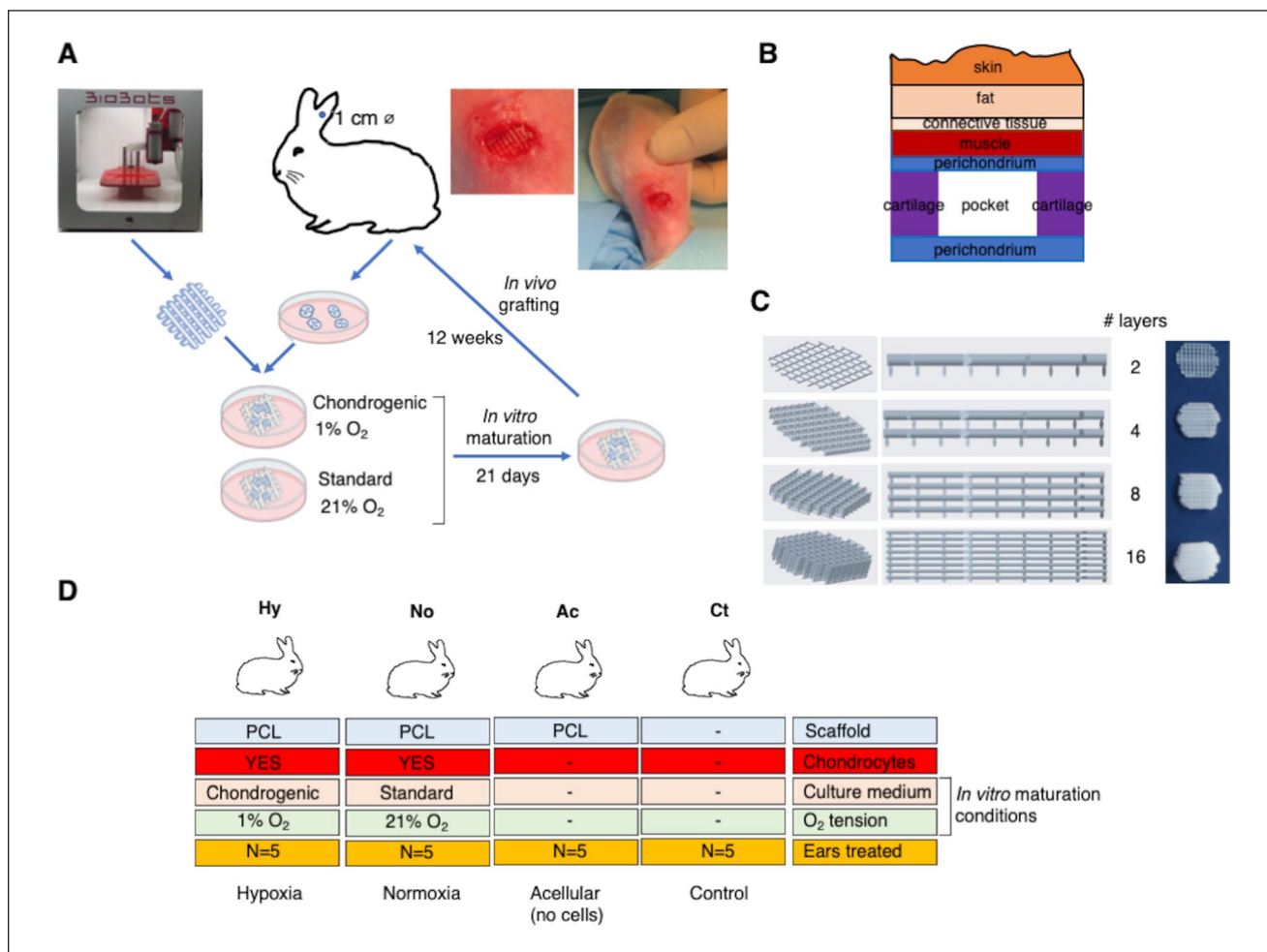


**Figure 1.** Experimental strategy and *in vivo* study groups. **(A)** PCL-based scaffolds were 3D-printed on a Biobots 1 bioprinter. Rabbit auricular chondrocytes were grown on the meshed structures and matured *in vitro* for 21 days in standard medium and normoxia or prochondrogenic medium and hypoxia. Matured constructs were grafted *in vivo* for 12 weeks on the generated defects as shown on the images. **(B)** Schematic structure of the “perichondrium pocket” defects. An incision was made to generate a defect in cartilage and introduce the scaffold within the generated pocket, which was surrounded at all sides by cartilage and perichondrium. **(C)** Design and examples of scaffolds composed of 2, 4, 8, and 16 layers. **(D)** *In vivo* study groups. Rabbits (*N* = 20) were divided into 4 experimental groups: *Hy* (grafted with cell-laden scaffolds in hypoxia), *No* (grafted with cell-laden scaffolds in normoxia), *Ac* (grafted with acellular scaffolds), and *Ct* (negative controls). PCL = polycaprolactone; 3D = 3-dimensional.

were only obtained between days 0 and 21 in hypoxic conditions (*P* = 0.026). These results suggested that adequate cell survival and differentiation were obtained in all culture conditions, with relatively minor improvements being provided by the culture of chondrocytes in prochondrogenic media and under hypoxic conditions.

**Chondrogenic gene expression in 3D scaffolds in vitro (RT-qPCR).** Chondrogenic differentiation may be quantitatively determined by measuring the expression of chondrogenic genes such as *COL1A1*, *COL2A1*, *SOX9*, *ACAN*, and *COL10A1* by RT-qPCR. Expression analysis at day 7, 14, and 21 of *in vitro* maturation culture revealed interesting

differences between the normoxia (*No*) and hypoxia (*Hy*) culture groups (**Fig. 3**). In normoxia, all 5 chondrogenic genes gradually decreased the expression in cultured scaffolds as cultures progressed. In contrast, in the case of hypoxic culture conditions, *ACAN*, *COL2A1*, and *SOX9* showed the same tendency but with a slower decrease due to increased overall levels, while *COL1A1* expression remained high until day 21 and *COL10A1* was virtually absent. Thus, chondrogenic genes were clearly increased in hypoxic conditions compared with normoxia, suggesting that the pro-chondrogenic medium and hypoxic condition were able to maintain a chondrogenic phenotype in culture better than standard chondrocyte expansion culture conditions.

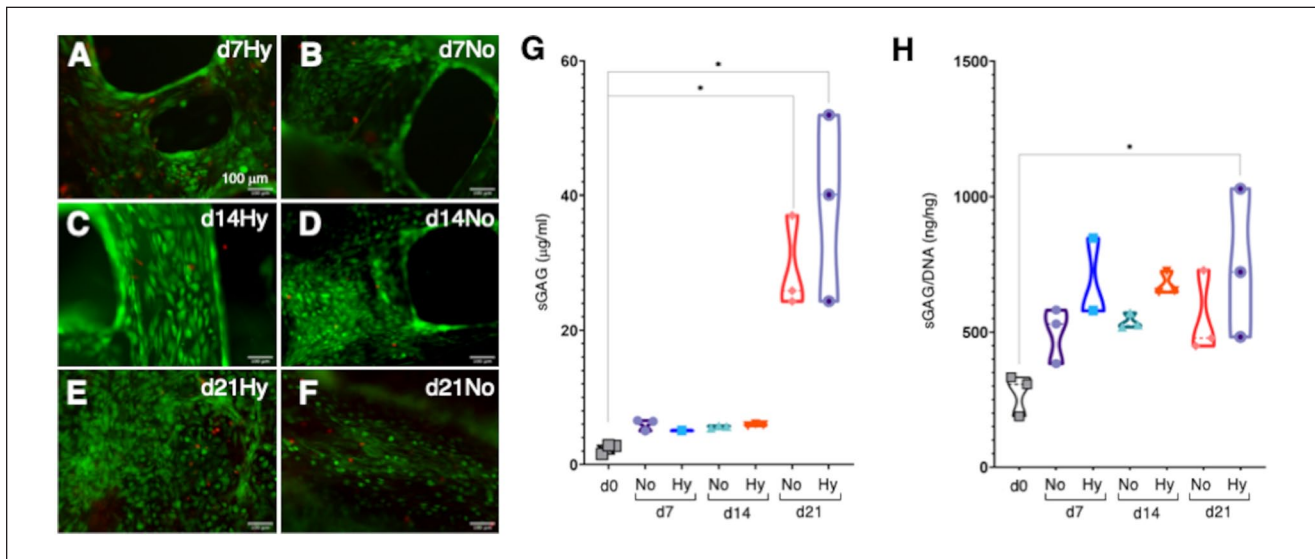


**Figure 2.** Cell viability and biochemical characterization of *in vitro* matured constructs. **(A-F)** Fluorescence microscope images showing chondrocytes growing on scaffolds. Live cells are shown in green (calcein AM), while non-viable cells are shown in red (ethidium homodimer). **(A, C, E)** Chondrocytes in culture with prochondrogenic medium and hypoxia on days 7, 14, and 21, respectively. **(B, D, F)** Chondrocytes grown on standard culture medium and normoxia on days 7, 14, and 21, respectively. Images correspond to an objective of 10x. **(G)** Quantitative assessment of sGAG production by chondrocytes growing on the constructs in normoxic/basal medium (No) versus hypoxic/prochondrogenic conditions (Hy) in days 0, 7, 14, and 21 of culture. **(H)** sGAG production normalized to DNA content by chondrocytes growing on the scaffolds in normoxic/basal medium (No) versus hypoxic/prochondrogenic conditions (Hy) in days 0, 7, 14, and 21 of culture. sGAG = sulfated glycosaminoglycans. \* $P < 0.05$ .

**Mechanical properties of neocartilage.** To determine the mechanical properties of the matured scaffolds, constructs cultivated in normoxia (No) and hypoxia (Hy) were compared in their performance in uniaxial compression tests to acellular scaffolds (Ac) and native rabbit ear cartilage (Fig. 4). Unfortunately, the roughness of the samples and the lack of homogeneity in their thickness made obtaining reliable results from the early stages of compression unfeasible. To minimize the effects of the settlement of the plates on the specimens, the elastic modulus, or Young's modulus, was determined as the slope in the stress-strain plots between strains of 0.075 and 0.1, that is, between a deformation of 7.5% and 10%. For each of the materials studied, the results of at least 8 specimens were averaged. Figure 4A shows an example of the load-strain records obtained for the studied materials. Dispersion of results were high. In the case of these 4 samples, the softest material corresponds to Native cartilage and the stiffest to the Ac sample. An average of 10.8 kPa elastic modulus was determined for native rabbit cartilage. As expected,<sup>5</sup> the stiffness of all artificial materials was far significantly superior to that of the natural material as can be seen in Figure 4B. The elastic modulus of hypoxia (Hy) specimen was 1,054 kPa ( $P < 0.001$ ), whereas normoxia (No) and Ac group specimens' values were 229 and 364 kPa, respectively ( $P < 0.05$ ). These results suggest that maturation of the scaffolds in hypoxic conditions yielded a significantly stiffer construct for transplantation.

**SEM analysis and immunofluorescence of the scaffolds.** SEM was performed to observe the scaffolds' microstructure and chondrocyte distribution (Fig. 5). Acellular PCL scaffolds (Ac) revealed apparent thickening of PCL fibers (Fig. 5A, Ac). Nevertheless, this structural modification did not affect chondrocytes attachment which was already visible at day 1 of culture (Fig. 5A, d1). At day 21 of culture in the case of normoxic conditions (Fig. 5A, d21No), a chondrocyte cell sheet or monolayer was appreciated around PCL lattice. In contrast, chondrocytes formed a dense layer in hypoxic conditions indicative of ECM deposition (Fig. 5A, d21Hy). To confirm this finding, immunofluorescence staining for collagen type I and II proteins was performed on d21 scaffolds (Fig. 5B). Both collagen types were detected apparently forming 2 separate layers of ECM folded over themselves under hypoxic conditions (Fig. 5B, d21Hy). In contrast, in normoxic conditions, collagens showed a mixed pattern of distribution along the cell sheet (Fig. 5B, d21No).

### In Vivo Transplantation Assays on Rabbit Ears

Perichondrium pockets were generated in rabbits' ears, and in the case of the control group ( $N = 5$  ears), the wound was closed untreated. In experimental groups, tissue void was refilled with acellular scaffolds ( $N = 5$ ), scaffolds with chondrocytes cultured in non-prochondrogenic conditions ( $N = 5$ ), and scaffolds with chondrocytes cultured in prochondrogenic

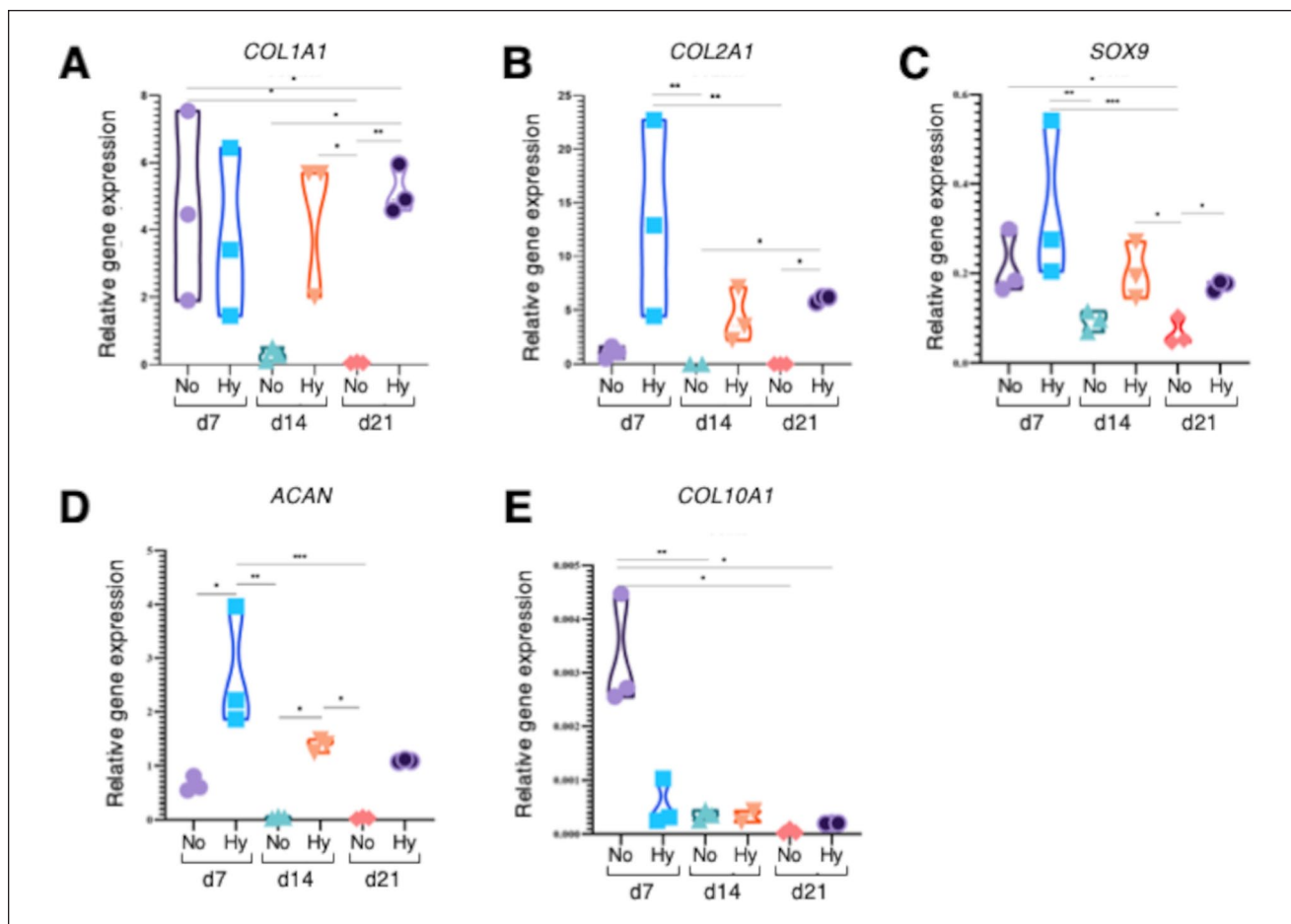


**Figure 3.** Chondrogenic gene expression profile by *in vitro* matured constructs. RT-qPCR analysis was done for chondrogenic markers such as collagen type I (*COL1A1*) (A), collagen type II (*COL2A1*) (B), *SOX9* (C), aggrecan (*ACAN*) (D), and collagen type X (*COL10A1*) (E). Experimental triplicates are shown for scaffolds grown in normoxic/basal medium (No) versus hypoxic/prochondrogenic conditions (Hy) at days 7, 14, and 21 of culture. Gene expression values ( $2^{-\Delta Ct}$ ) are shown relative to *GAPDH* housekeeping gene expression. RT-qPCR = reverse transcription-quantitative polymerase chain reaction. \* $P < 0.05$ , \*\* $P < 0.01$ , \*\*\* $P < 0.001$ .

conditions ( $N = 5$ ; Fig. 1D). The PCL cellular and acellular scaffolds located in the sub-perichondral pocket were well-tolerated by the animals, with no minor or major complications. In addition, CRP and procalcitonin serum levels showed no variation (data not shown), indicative of absence of a detectable inflammatory response to the grafts. At study end point, 20 specimens from the *in vivo* study were analyzed.

**Chondrogenic gene expression (RT-qPCR) in 3D scaffolds after *in vivo* implantation.** Chondrogenic gene expression (*COL1A1*, *COL2A1*, *ACAN*, *SOX9*, and *COL10A1*) was evaluated in extracted constructs after 12 weeks of transplantation, in the following groups: acellular scaffolds (*Ac*), scaffolds with cells grown in basal conditions in normoxia (*No*), and scaffolds with cells grown in prochondrogenic hypoxic conditions (*Hy*) (Fig. 6). RT-qPCR values were normalized to the control group without scaffold (*Ct*), which was used as a reference (Fig. 6A). All genes with the possible

exception of *COL1A1* showed no apparent increase compared with the *Ct* group. Similar to the results obtained at the *in vitro* maturation stage, *COL1A1*, *COL2A1*, *ACAN*, and *SOX9* expressions showed a tendency to increase in hypoxic conditions compared with normoxia (non-significant, Fig. 6A). However, acellular constructs (*Ac*) showed similarly high levels of chondrogenic gene expression, indicating that endogenous cell colonization of the constructs was significant. Of note, the expression of *COL10A1*, a marker of early calcification and hypertrophic chondrocytes,<sup>37</sup> was apparently increased in the *Ac* group, indicating that cell-laden constructs might provide a more suitable environment for proper cartilage formation.

**Histological evaluation and immunofluorescence analysis of the neocartilage formation *in vivo*.** At the 12-week end point of study, Alcian Blue-Safranin O staining was performed on extracted tissue sections (Fig. 6B-F and H). No

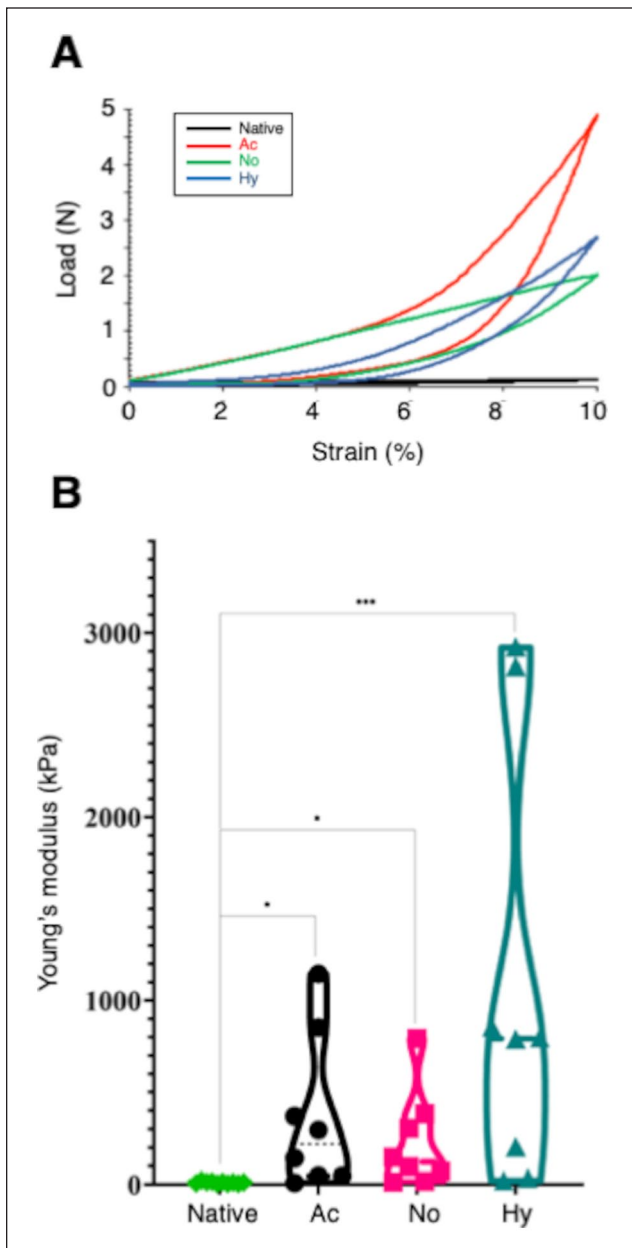


**Figure 4.** Biomechanical analysis of *in vitro* matured constructs. **(A)** Example of 4 load-strain records for native rabbit ear cartilage (*Native*, black), acellular scaffolds (*Ac*, red), cell-laden scaffolds with chondrocytes cultivated in normoxia (*No*, green), and cell-laden scaffolds with chondrocytes cultivated in hypoxia (*Hy*, blue). **(B)** Young's modulus values (kPa) measured for each material. \* $P < 0.05$ , \*\*\* $P < 0.001$ .

accumulation of collagen or GAGs was evident in *Ct-* or *Ac-*grafted control groups (Fig. 6B and C). Interestingly, the normoxia cell-laden scaffold (*No*) group showed a similar lack of apparent neocartilage differentiation (Fig. 6D and D'). In contrast, these analyses revealed significant neocartilage formation in scaffolds cultured under

prochondrogenic hypoxia (*Hy*) conditions (Fig. 6E and E'). Furthermore, the expression of collagen type I and II proteins was also confirmed by immunofluorescence analysis of sections of the *Hy* condition, which showed dense collagen deposition and lacunae surrounding the chondrocytes (Fig. 6H and I). These structures were visually comparable to those of the native cartilage tissue (Fig. 6F and G), although structurally more disorganized.

## Discussion

Due to its relative low cost and easiness of use, fused filament fabrication method represents nowadays one of the most used methods for 3D-printed scaffold fabrication, presenting a wide variety of available biomaterials.<sup>38,39</sup> Here, we confirmed the feasibility of transplanting a chondrocyte-laden, 2-layered PCL scaffold to an acute cartilage defect on rabbit ears. In this study, our main goal was to improve maturation of the constructs prior to transplantation and ideally emulate hyaline cartilage structure. Of note, as recently demonstrated by Hou *et al.*,<sup>40</sup> at least in the case of MSC-laden scaffolds, the native cartilage niche at the implantation site has a dominant role in cartilage type specification, that is, in the long-term, it does specify which specific types of cartilage will be generated from the implanted cell-laden constructs. In our study, we chose the perichondrium pocket in rabbit ear because it is structurally similar to nasoseptal cartilage, whose defects are clinically relevant. We also used auricular chondrocytes because, in our opinion, it is a more suitable source for clinical use than chondrocytes originating from nasoseptal biopsies. Thus, with regard to potential future use of these scaffolds in nasal septal cartilage reconstruction, we believe that other elastic or hyaline-like cartilage (e.g. auricle, meniscus) could be convenient sources of cells for autologous use in the clinic.

Primary chondrocytes cultured both under standard normoxic expansion and prochondrogenic hypoxic conditions showed detectable deposition of sGAG and type I and II collagens. *In vitro*, cartilage-like ECM deposition was most clear in the hypoxia prochondrogenic group. SEM images confirmed the secretion of a compact proteoglycan-based matrix in matured scaffolds, composed of collagen types I and II as revealed by immunofluorescence. RT-qPCR experiments revealed lower expression of chondrogenic markers in standard expansion conditions compared with the hypoxia group. Wongin *et al.*<sup>41</sup> have argued that 2D cell growth induces stress fiber formation, lowering Sox9 production by blocking RhoA signaling. In contrast, prochondrogenic hypoxia conditions in our study may have provided a thick and dense ECM layer in which chondrocytes mimicked their round shape at the native niche, which perhaps promoted an improved retention of the expression of cartilage markers.



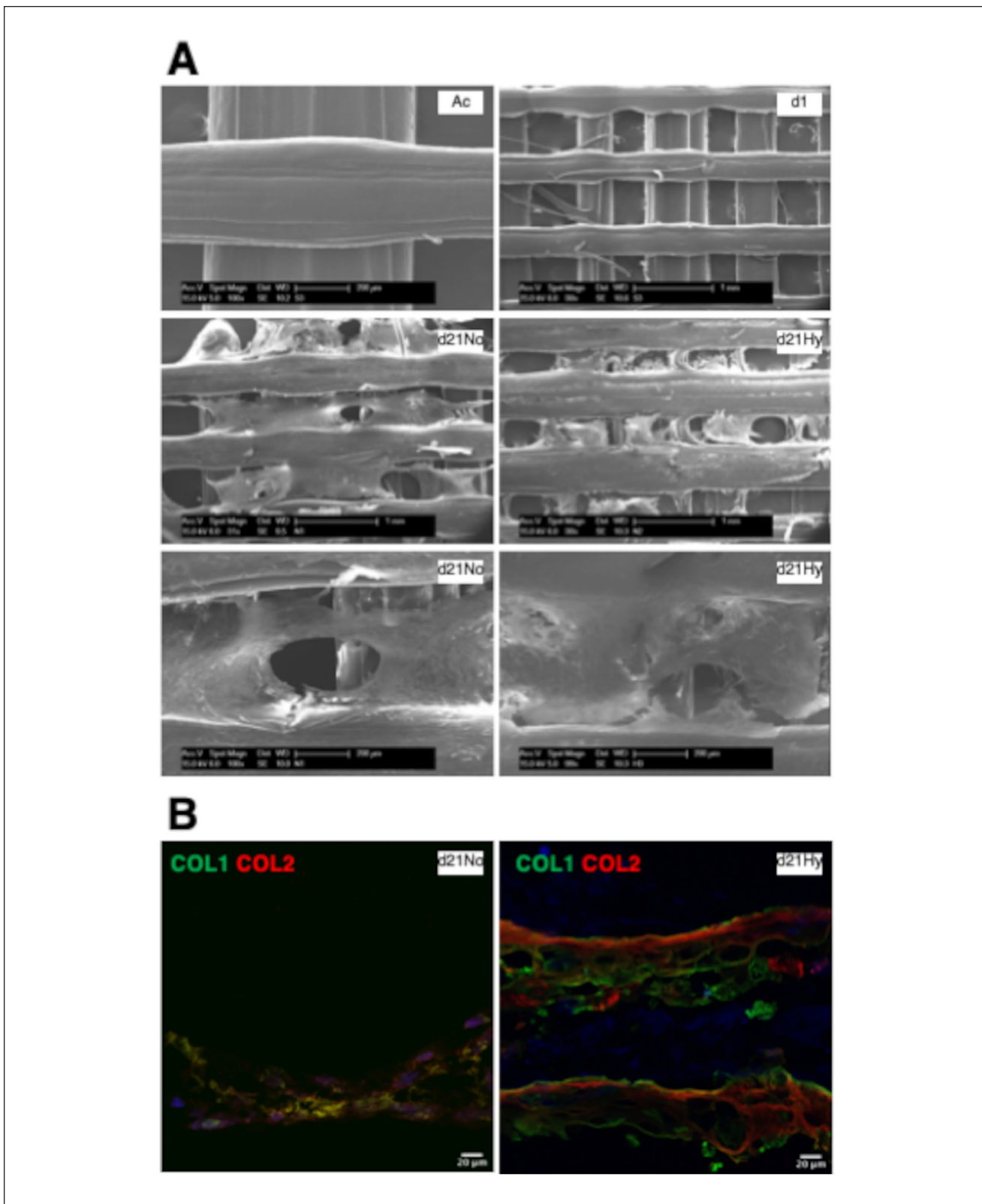


**Figure 5.** Ultrastructural characterization of *in vitro* matured constructs. **(A)** Scanning electron microscopy images of acellular scaffolds (Ac), cell-laden scaffolds cultivated for 1 day (d1), cell-laden scaffolds with chondrocytes cultivated for 21 days in normoxia (No), and cell-laden scaffolds with chondrocytes cultivated for 21 days in hypoxia (Hy). Ac and d1 images were taken in normoxia. **(B)** Representative immunofluorescence images of collagen type I (COL1, green) and collagen type II (COL2, red) are shown for chondrocytes grown in standard-normoxic (No) and chondrogenic-hypoxic conditions (Hy) at day 21 of culture.

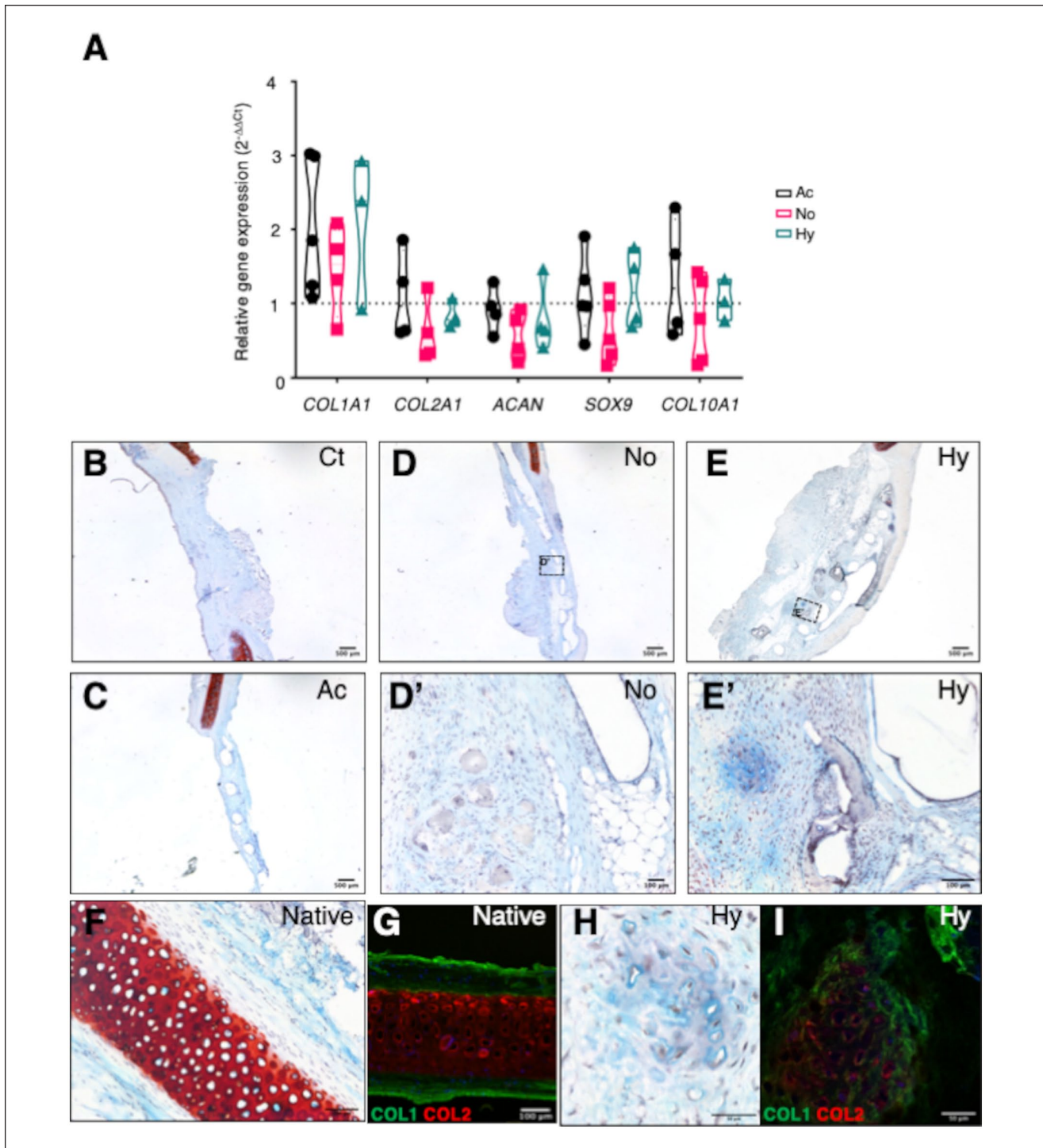


**Figure 6.** Gene expression and histological analyses of grafted constructs at the end point of *in vivo* study. **(A)** Chondrogenic gene expression after 12 weeks of *in vivo* experiment on rabbit ears. RT-qPCR analysis was done for chondrogenic markers such as collagen type I (*COL1A1*), collagen type II (*COL2A1*), aggrecan (*ACAN*), *SOX9*, and collagen type X (*COL10A1*). Experimental triplicates are shown for acellular scaffolds (Ac, black), scaffolds grown in normoxic/basal medium (No, red), and hypoxic/prochondrogenic conditions (Hy, green). Gene expression values ( $2^{-\Delta\Delta Ct}$ ) are shown relative to negative control (Ct) group. **(B-I)** Histological evaluation of the cartilage after 12 weeks of *in vivo* experiment. Examples of Safranin O and immunofluorescence staining of each group of treatment, controls, and native tissue are represented. **(B)** Control group (Ct). **(C)** Acellular scaffold (Ac). **(D, D')** Normoxic scaffold (No). **(E, E')** Hypoxic scaffold (Hy). **(F, G)** Native rabbit ear cartilage (Native). **(H, I)** Hypoxic scaffold (Hy). Representative immunofluorescence images of collagen type I (COL1, green) and collagen type II (COL2, red) are shown in panels **G** and **I**. RT-qPCR = reverse transcription-quantitative polymerase chain reaction.

Histological analyses performed on scaffolds extracted of the *in vivo* experiments demonstrated again the presence of collagen types I and II as well as cartilage regeneration. These are the major collagens in cartilage. Type II collagen is primarily found in hyaline cartilage (such as articular and nasal septal cartilage) and is considered the first choice as a cartilage substitute in many surgical procedures.<sup>42</sup> Unfortunately, type II collagen shows unwanted arthritogenic activities.<sup>43,44</sup> By contrast, type I collagen does not elicit adverse immune reaction particularly in the absence of its telopeptides, and lacks arthritogenic effects.<sup>45,46</sup> In addition, due to its higher biocompatibility, type I collagen is used commonly in cartilage tissue engineering.<sup>47</sup>

Collagen type I is the main fibrillar type of fibrocartilage and elastic cartilage. The highest presence of *COL1A1* mRNA *in vivo* might indicate the presence of elastic cartilage, by dominance of the receptor site, or dedifferentiation of the implanted chondrocyte pool. From RT-qPCR data obtained in the *in vitro* assays, the expression of collagen I was maintained in the case of scaffolds subjected to pro-chondrogenic differentiation in hypoxia, suggesting partial dedifferentiation as argued by Rampichová *et al.*<sup>48</sup> Histologically, we observed clear neocartilage formation after 12 weeks *in vivo*. In addition, a high percentage of the cross-sectional area was occupied by GAG surrounding cells, and immunostaining demonstrated type II collagen deposition, with cluster formation of collagen II positive cells surrounded by a collagen I matrix. These results can be considered as a qualitative evidence of cartilage-like tissue formation over the 3D-printed scaffolds.

With regard to mechanical properties of the matured scaffolds, Young's modulus of printed scaffolds was higher than the rabbits' ear native cartilage. According to bibliography, the elastic modulus of human nasal septal cartilage presents values of  $2.72 \pm 0.82$  MPa<sup>49</sup> that could be in line with the values obtained for hypoxia group in our study ( $1.054 \pm 0.41$  MPa). The absence of complications like extrusions or skin erosions in this subset of animals may be related to the relatively short follow-up. We are currently running long-term follow-up studies to evaluate the behavior of scaffolds in 6- and 12-month periods. In a second study currently in progress, we are now cultivating human nasal septal chondrocytes to create a human 3D-printed nasal septal cartilage substitute that will be tested in pre-clinical studies.

In addition to the aforementioned, a number of strategies could be used to further improve *in vitro* chondrogenic differentiation and possibly shorten the time required for scaffold maturation. On the cellular side, chondrocyte-derived extracellular vesicles immobilized onto electrospun PCL nanofibers have been shown to promote chondrogenic cell fate.<sup>50</sup> Co-cultures of MSCs and primary chondrocytes seem to enhance differentiation properties in a synergistic manner.<sup>51</sup> Similarly, the use of coatings based on decellularized hyaline cartilage ECM promotes chondrogenic

differentiation of periosteal cells.<sup>52</sup> On the materials side, pore geometry and size could be tailored to improve chondrogenic differentiation properties.<sup>53,54</sup> Cartilage-derived ECM could also be included on composite material formulations.<sup>55</sup> Finally, use of more biomimetic microenvironments such as application of dynamic compression forces may further improve functional graft characteristics.<sup>56</sup>

## Conclusions

*In vitro* maturation of engineered cartilage scaffolds under prochondrogenic conditions that better mimic the *in vivo* environment may be beneficial to improve functional properties of the engineered grafts. The proposed maturation strategy may also be of use for other tissue-engineered constructs and may ultimately impact survival and integration of the grafts<sup>57</sup> in the damaged tissue microenvironment.<sup>58</sup>

## Acknowledgments and Funding

We acknowledge the excellent technical assistance of Edurne Bereciartua from the Biochemistry Service of OSI Donostialdea-Donostia University Hospital. The author(s) disclosed receipt of the following financial support for the research, authorship and/or publication of this article: National grants from Instituto de Salud Carlos III (ISCIII) through the projects PI16/01430, PI19/01621, and PT20/00030 and, co-funded by the European Union (EU); grants from the Department of Health (17BU207, 19BU203, 20BU206, 20BU210, 2020111004, 21BU203) and the Department of Economy and Competitiveness of the Basque Government (KK-2020/00010, KK-2019/00006, KK-2019/00093); and Diputación Foral de Gipuzkoa. R.H.-M. was supported by the ISCIII Platform Biobanks and Biomodels, PT20/00030, co-funded by the EU



## Declaration of Conflicting Interests

The author(s) declared no potential conflicts of interest with respect to the research, authorship, and/or publication of this article.

## Ethical Approval

The Biodonostia Animal Care Committee, Authorized Body, and Competent Authority approved the animal experimentation reported in this study with reference numbers CEEA 19/001, OH19/001, and PRO-AE-SS-131, respectively, in accordance with Spanish Royal Decree 1386/2018, European Directive 2010/63/EU, and other relevant guidelines.

## ORCID iDs

Raquel Hernández-Moya  <https://orcid.org/0000-0002-8684-8306>  
Ander Izeta  <https://orcid.org/0000-0003-1879-7401>

## References

1. Wiggenhauser PS, Schantz JT, Rotter N. Cartilage engineering in reconstructive surgery: auricular, nasal and tracheal engineering from a surgical perspective. *Regen Med.* 2017;12(3):303-14. doi:10.2217/rme-2016-0160.

2. Wei W, Dai H. Articular cartilage and osteochondral tissue engineering techniques: recent advances and challenges. *Bioact Mater*. 2021;6(12):4830-55. doi:10.1016/j.bioactmat.2021.05.011.
3. Zhao X, Hu DA, Wu D, He F, Wang H, Huang L, *et al*. Applications of biocompatible scaffold materials in stem cell-based cartilage tissue engineering. *Front Bioeng Biotechnol*. 2021;9:603444. doi:10.3389/fbioe.2021.603444.
4. Beketov EE, Isaeva EV, Shegay PV, Ivanov SA, Kaprin AD. Current state of tissue engineering for cartilage regeneration. *Genes Cells*. 2019;14(2):12-20. doi:10.23868/201906013.
5. Lavernia L, Brown WE, Wong BJF, Hu JC, Athanasiou KA. Toward tissue-engineering of nasal cartilages. *Acta Biomater*. 2019;88:42-56. doi:10.1016/j.actbio.2019.02.025.
6. Shen S, Chen M, Guo W, Li H, Li X, Huang S, *et al*. Three dimensional printing-based strategies for functional cartilage regeneration. *Tissue Eng Part B Rev*. 2019;25(3):187-201. doi:10.1089/ten.TEB.2018.0248.
7. Raut AV, Agrawal A, Bagde A, Fulzele P, Quazi Syed Z. 3-D Bioprinting in cartilage tissue engineering for bioinks-short review. *Mater Today Proc*. Published online 17 June 2021. doi:10.1016/j.matpr.2021.05.625.
8. Tiwari D, Vobilisetty RK, Heer B. Current application and future prospects of 3D printing in otorhinolaryngology—a narrative review. *Indian J Otolaryngol Head Neck Surg*. 2022;74(1):123-6. doi:10.1007/s12070-021-02634-5.
9. Cao Y, Sang S, An Y, Xiang C, Li Y, Zhen Y. Progress of 3D printing techniques for nasal cartilage regeneration. *Aesthetic Plast Surg*. 2022;46(2):947-64. doi:10.1007/s00266-021-02472-4.
10. Agarwal T, Chiesa I, Presutti D, Irawan V, Vajanthri KY, Costantini M, *et al*. Recent advances in bioprinting technologies for engineering different cartilage-based tissues. *Mater Sci Eng C Mater Biol Appl*. 2021;123:112005. doi:10.1016/j.msec.2021.112005.
11. Huang J, Xiong J, Wang D, Zhang J, Yang L, Sun S, *et al*. 3D bioprinting of hydrogels for cartilage tissue engineering. *Gels*. 2021;7(3):144. doi:10.3390/gels7030144.
12. Messaoudi O, Henrionnet C, Bourge K, Loeuille D, Gillet P, Pinzano A. Stem cells and extrusion 3D printing for hyaline cartilage engineering. *Cells*. 2021;10(1):2. doi:10.3390/cells10010002.
13. Chiesa-Estomba CM, Aiastui A, González-Fernández I, Hernández-Moya R, Rodiño C, Delgado A, *et al*. Three-dimensional bioprinting scaffolding for nasal cartilage defects: a systematic review. *Tissue Eng Regen Med*. 2021;18(3):343-53. doi:10.1007/s13770-021-00331-6.
14. Roseti L, Cavallo C, Desando G, Parisi V, Petretta M, Bartolotti I, *et al*. Three-dimensional bioprinting of cartilage by the use of stem cells: a strategy to improve regeneration. *Materials*. 2018;11(9):1749. doi:10.3390/ma11091749.
15. Wu Y, Kennedy P, Bonazza N, Yu Y, Dhawan A, Ozbolat I. Three-dimensional bioprinting of articular cartilage: a systematic review. *Cartilage*. 2021;12(1):76-92. doi:10.1177/1947603518809410.
16. Niermeyer WL, Rodman C, Li MM, Chiang T. Tissue engineering applications in otolaryngology—the state of translation. *Laryngoscope Investig Otolaryngol*. 2020;5(4):630-48. doi:10.1002/lio2.416.
17. Backes EH, Harb SV, Beatrice CAG, Shimomura KMB, Passador FR, Costa LC, *et al*. Polycaprolactone usage in additive manufacturing strategies for tissue engineering applications: a review. *J Biomed Mater Res B Appl Biomater*. 2022;110(6):1479-503. doi:10.1002/jbm.b.34997.
18. Kim JH, Kim GW, Kang WK. Nasal tip plasty using three-dimensional printed polycaprolactone (Smart Ball®). *Yeungnam Univ J Med*. 2020;37(1):32-9. doi:10.12701/yujm.2019.00290.
19. Yap E. Techniques in the safe use of polycaprolactone in structural rhinoplasty. *Philippine J Otolaryngol Head Neck Surg*. 2020;35(1):66-70. doi:10.32412/pjohns.v35i1.1267.
20. Hashimdeen SH, Thorogate R, Miodownik M, Edirisinghe MJ. Fabrication of bespoke nasal septal scaffolds. *Mater Des*. 2016;90:403-9. doi:10.1016/j.matdes.2015.10.120.
21. Kim DH, Lee IH, Yun WS, Shim JH, Choi D, Hwang SH, *et al*. Long-term efficacy and safety of 3D printed implant in patients with nasal septal deformities. *Eur Arch Otorhinolaryngol*. 2022;279(4):1943-50. doi:10.1007/s00405-021-06996-y.
22. Ibragimova SI, Medvedeva E, Romanova IA, Istranov LP, Istranova EV, Lychagin AV, *et al*. Implantation of various cell-free matrixes does not contribute to the restoration of hyaline cartilage within full-thickness focal defects. *Int J Mol Sci*. 2022;23(1):292. doi:10.3390/ijms23010292.
23. Izgordu MS, Uzgur EI, Ulag S, Sahin A, Karademir Yilmaz B, Kilic B, *et al*. Investigation of 3D-printed polycaprolactone-/polyvinylpyrrolidone-based constructs. *Cartilage*. 2021;13(Suppl 2):626S-635S. doi:10.1177/1947603519897302.
24. Evenbratt H, Andreasson L, Bicknell V, Brittberg M, Mobini R, Simonsson S. Insights into the present and future of cartilage regeneration and joint repair. *Cell Regen*. 2022;11(1):3. doi:10.1186/s13619-021-00104-5.
25. Rikkers M, Korpershoek JV, Levato R, Malda J, Vonk LA. The clinical potential of articular cartilage-derived progenitor cells: a systematic review. *NPJ Regen Med*. 2022;7(1):2. doi:10.1038/s41536-021-00203-6.
26. Liang Y, Szojka ARA, Idrees E, Kunze M, Mulet-Sierra A, Adesida AB. Re-differentiation of human meniscus fibrochondrocytes differs in three-dimensional cell aggregates and decellularized human meniscus matrix scaffolds. *Ann Biomed Eng*. 2020;48(3):968-79. doi:10.1007/s10439-019-02272-7.
27. Kafienah W, Jakob M, Démarteau O, Frazer A, Barker MD, Martin I, *et al*. Three-dimensional tissue engineering of hyaline cartilage: comparison of adult nasal and articular chondrocytes. *Tissue Eng*. 2002;8(5):817-26. doi:10.1089/10763270260424178.
28. Campbell TM, Dilworth FJ, Allan DS, Trudel G. The hunt is on! In pursuit of the ideal stem cell population for cartilage regeneration. *Front Bioeng Biotechnol*. 2022;10:866148. doi:10.3389/fbioe.2022.866148.
29. Blum JC, Schenck TL, Birt A, Giunta RE, Wigenhauser PS. Artificial decellularized extracellular matrix improves the regenerative capacity of adipose tissue derived stem cells on 3D printed polycaprolactone scaffolds. *J Tissue Eng*. 2021;12:1-12. doi:10.1177/20417314211022242.

30. San-Marina S, Sharma A, Voss SG, Janus JR, Hamilton GS. Assessment of scaffolding properties for chondrogenic differentiation of adipose-derived mesenchymal stem cells in nasal reconstruction. *JAMA Facial Plast Surg.* 2017;19(2):108-14. doi:10.1001/jamafacial.2016.1200.
31. Zhou S, Chen S, Jiang Q, Pei M. Determinants of stem cell lineage differentiation toward chondrogenesis versus adipogenesis. *Cell Mol Life Sci.* 2019;76(9):1653-80. doi:10.1007/s00018-019-03017-4.
32. Kim DH, Lim MH, Jeun JH, Park SH, Lee W, Park SH, et al. Evaluation of polycaprolactone-associated human nasal chondrocytes as a therapeutic agent for cartilage repair. *Tissue Eng Regen Med.* 2019;16(6):605-14. doi:10.1007/s13770-019-00210-1.
33. Kundu J, Shim JH, Jang J, Kim SW, Cho DW. An additive manufacturing-based PCL-alginate-chondrocyte bioprinted scaffold for cartilage tissue engineering. *J Tissue Eng Regen Med.* 2015;9(11):1286-97. doi:10.1002/term.1682.
34. Lan X, Liang Y, Erkut EJN, Kunze M, Mulet-Sierra A, Gong T, et al. Bioprinting of human nasoseptal chondrocytes-laden collagen hydrogel for cartilage tissue engineering. *FASEB J.* 2021;35(3):e21191. doi:10.1096/fj.202002081R.
35. Yin Z, Li D, Liu Y, Feng S, Yao L, Liang X, et al. Regeneration of elastic cartilage with accurate human-ear shape based on PCL strengthened biodegradable scaffold and expanded microtia chondrocytes. *Appl Mater Today.* 2020;20:100724. doi:10.1016/j.apmt.2020.100724.
36. Lohan A, Marzahn U, El Sayed K, Haisch A, Kohl B, Müller RD, et al. In vitro and in vivo neo-cartilage formation by heterotopic chondrocytes seeded on PGA scaffolds. *Histochem Cell Biol.* 2011;136(1):57-69. doi:10.1007/s00418-011-0822-2.
37. Togo T, Utani A, Naitoh M, Ohta M, Tsuji Y, Morikawa N, et al. Identification of cartilage progenitor cells in the adult ear perichondrium: utilization for cartilage reconstruction. *Lab Invest.* 2006;86(5):445-57. doi:10.1038/labinvest.3700409.
38. Park SH, Yun BG, Won JY, Yun WS, Shim JH, Lim MH, et al. New application of three-dimensional printing biomaterial in nasal reconstruction. *Laryngoscope.* 2017;127(5):1036-43. doi:10.1002/lary.26400.
39. Kim YS, Shin YS, Park DY, Choi JW, Park JK, Kim DH, et al. The application of three-dimensional printing in animal model of augmentation rhinoplasty. *Ann Biomed Eng.* 2015;43(9):2153-62. doi:10.1007/s10439-015-1261-3.
40. Hou M, Tian B, Bai B, Ci Z, Liu Y, Zhang Y, et al. Dominant role of in situ native cartilage niche for determining the cartilage type regenerated by BMSCs. *Bioact Mater.* 2022;13:149-60. doi:10.1016/j.bioactmat.2021.11.007.
41. Wongin S, Waikakul S, Chotiyanwong P, Siriwatwechakul W, Viravaidya-Pasuwat K. Effect of cell sheet manipulation techniques on the expression of collagen type II and stress fiber formation in human chondrocyte sheets. *Tissue Eng Part A.* 2018;24(5-6):469-78. doi:10.1089/ten.TEA.2017.0013.
42. Gudmann NS, Karsdal MA. Type II collagen. In: Karsdal MA, editor. *Biochemistry of collagens, laminins and elastin.* Academic Press; 2016. p. 13-20. doi:10.1016/B978-0-12-809847-9.00002-7.
43. Trentham DE, Townes AS, Kang AH. Autoimmunity to type II collagen: an experimental model of arthritis. *J Exp Med.* 1977;146(3):857-68. doi:10.1084/jem.146.3.857.
44. Yoo TJ, Stuart JM, Takeda T, Sudo N, Floyd RA, Ishibe T, et al. Induction of type II collagen autoimmune arthritis and ear disease in monkey. *Ann N Y Acad Sci.* 1986;475(1):341-2. doi:10.1111/j.1749-6632.1986.tb20886.x.
45. Lynn AK, Yannas IV, Bonfield W. Antigenicity and immunogenicity of collagen. *J Biomed Mater Res B Appl Biomater.* 2004;71(2):343-54. doi:10.1002/jbm.b.30096.
46. Radhakrishnan S, Nagarajan S, Bechelany M, Kalkura SN. Collagen based biomaterials for tissue engineering applications: a review. In: *Lecture notes in earth system sciences.* 2020. doi:10.1007/978-3-030-21614-6\_1.
47. Irawan V, Sung TC, Higuchi A, Ikoma T. Collagen scaffolds in cartilage tissue engineering and relevant approaches for future development. *Tissue Eng Regen Med.* 2018;15(6):673-97. doi:10.1007/s13770-018-0135-9.
48. Rampichová M, Košťáková Kuželová E, Filová E, Chvojka J, Šafka J, Pelcl M, et al. Composite 3D printed scaffold with structured electrospun nanofibers promotes chondrocyte adhesion and infiltration. *Cell Adh Migr.* 2018;12(3):271-85. doi:10.1080/19336918.2017.1385713.
49. Griffin MF, Premakumar Y, Seifalian AM, Szarko M, Butler PE. Biomechanical characterisation of the human nasal cartilages; implications for tissue engineering. *J Mater Sci Mater Med.* 2016;27(1):11. doi:10.1007/s10856-015-5619-8.
50. Casanova MR, Osório H, Reis RL, Martins A, Neves NM. Chondrogenic differentiation induced by extracellular vesicles bound to a nanofibrous substrate. *NPJ Regen Med.* 2021;6(1):79. doi:10.1038/s41536-021-00190-8.
51. Posniak S, Chung JHY, Liu X, Mukherjee P, Gambhir S, Khansari A, et al. Bioprinting of chondrocyte stem cell co-cultures for auricular cartilage regeneration. *ACS Omega.* 2022;7(7):5908-20. doi:10.1021/acsomega.1c06102.
52. Vas WJ, Shah M, Roberts HC, Roberts SJ. Decellularised cartilage ECM culture coatings drive rapid and robust chondrogenic differentiation of human periosteal cells. *Bioengineering.* 2022;9(5):203. doi:10.3390/bioengineering9050203.
53. Martínez-Moreno D, Jiménez G, Chocarro-Wrona C, Carrillo E, Montañez E, Galocha-León C, et al. Pore geometry influences growth and cell adhesion of infrapatellar mesenchymal stem cells in biofabricated 3D thermoplastic scaffolds useful for cartilage tissue engineering. *Mater Sci Eng C Mater Biol Appl.* 2021;122:111933. doi:10.1016/j.msec.2021.111933.
54. Theodoridis K, Aggelidou E, Vavilis T, Manthou ME, Tsimponis A, Demiri EC, et al. Hyaline cartilage next generation implants from adipose-tissue-derived mesenchymal stem cells: comparative study on 3D-printed polycaprolactone scaffold patterns. *J Tissue Eng Regen Med.* 2019;13(2):342-55. doi:10.1002/term.2798.
55. Zare P, Pezeshki-Modaress M, Davachi SM, Chahsetareh H, Simorgh S, Asgari N, et al. An additive manufacturing-based 3D printed poly  $\epsilon$ -caprolactone/alginate sulfate/extracellular matrix construct for nasal cartilage regeneration. *J Biomed Mater Res A.* 2022;110(6):1199-209. doi:10.1002/jbm.a.37363.

56. Remya NS, Nair PD. Matrix remodeling and mechanotransduction in in vitro chondrogenesis: implications towards functional stem cell-based cartilage tissue engineering. *Eng Rep.* 2020;2(5):e12145. doi:10.1002/eng2.12145.
57. Yari D, Ebrahimzadeh MH, Movaffagh J, Shahroodi A, Shirzad M, Qujeq D, *et al.* Biochemical aspects of scaffolds for cartilage tissue engineering; from basic science to regenerative medicine. *Arch Bone Jt Surg.* 2022;10(3):229-44. doi:10.22038/ABJS.2022.55549.2766.
58. Li M, Yin H, Yan Z, Li H, Wu J, Wang Y, *et al.* The immune microenvironment in cartilage injury and repair. *Acta Biomater.* 2022;140:23-42. doi:10.1016/j.actbio.2021.12.006.